PCCP

ROYAL SOCIETY OF CHEMISTRY

PAPER

View Article Online
View Journal | View Issue





Cite this: *Phys. Chem. Chem. Phys.*, 2022, **24**, 26144

# Spontaneous mirror symmetry breaking in reaction–diffusion systems: ambivalent role of the achiral precursor†

Jean Gillet, * Laurence Rongy and Yannick De Decker

Received 7th July 2022,
Accepted 14th October 2022

DOI: 10.1039/d2cp03102g

rsc.li/pccp

The behaviour of a Frank-like chemical network model featuring autocatalytic production of chiral enantiomers from achiral reactants is studied numerically in 1D and 2D systems using fluctuating initial conditions and accounting for diffusion processes. Our results reveal that the achiral substrate concentration can play an ambivalent role. It is shown that when the achiral reactant concentration is maintained constant and homogeneous in 1D systems, global homochirality is not systematically reached when the size of the system or the achiral reactant concentration are increased. However, with a fixed concentration gradient, coexisting homochiral domains of opposite handedness are no longer observed and homogeneous homochirality, *i.e.* the presence of a single stable homochiral domain, is recovered. In 2D systems, reaching global homochirality is just a matter of time. This time is dramatically increased when insufficient or excessive amount of achiral reactant is used. An optimal amount of achiral material is observed to maximise the enantiomer production rates.

## 1 Introduction

Since the discovery of chirality by Pasteur in the 19th century,[1] the emergence of homochirality (*i.e.*, of systems containing a single enantiomer) has remained an intriguing phenomenon. The question of the origin of homochirality is especially relevant in the context of the emergence of life.[2] Unravelling the mechanisms leading to homochirality could explain, for example, why most amino acids in living systems are found in their left-handed form, whereas the deoxyribose in DNA is in its right-handed form.

The emergence of such an asymmetry is expected to follow a general two-stage process. First, a chiral bias is spontaneously created or introduced in the system and second, an amplification of this bias allows reaching a homochiral composition.[3] In this context, spontaneous mirror symmetry breaking (SMSB) is the most commonly accepted scenario for the emergence of homochirality in experimental systems and nature.[4] SMSB is thought to occur whenever the racemic composition of a system becomes unstable and is spontaneously replaced by a stable, non-racemic state.

Numerous experiments and theoretical works have been conducted to understand the mechanisms leading to SMSB and to design systems where it could be induced and controlled.[4–7] SMSB was first observed during crystallisation experiments in the early 1990s.[8] A stirred solution of $NaClO_3$, which precipitates as an enantiomeric conglomerate, exhibited SMSB where the selection of the amplified enantiomer was arbitrary. Later, Viedma showed that the complete deracemisation of a racemic mixture of $NaClO_3$ crystals can be reached by stirring in the presence of glass beads.[9–11] The beads are expected to play a central role in the observed SMSB: they induce the fragmentation of larger crystals into smaller ones, which leads to an autocatalytic production of conglomerates. This so-called "Viedma ripening", was a big step forward towards the implementation of a reliable resolution method for crystals and a true proof of concept for the special role played by non-linearity in chiral symmetry breaking. A few years later, Viedma *et al.* extended this procedure to intrinsically chiral molecules, with the observation of a significant increase of the enantiomeric excess for a proteinogenic amino acid.[12] The Viedma ripening has found many applications,[13] such as the complete deracemisation of pharmaceutical molecules[14,15] or the enantio enrichment in organic reactions based on chiral or achiral compounds.[11,16–18]

Soai's reaction was the first demonstration of SMSB in chemical reactions and consists in an asymmetric autocatalysis in organic synthesis.[19,20] This reaction corresponds to an alkylation of aldehydes, during which two achiral reactants form a chiral product. As the reaction proceeds, the initial excess of one enantiomer, either created by an external source or introduced as an initial bias, is amplified.[19] An almost

*Nonlinear Physical, Chemistry Unit, CP-231, Université libre de Bruxelles (ULB), 1050 Bruxelles, Belgium. E-mail: Jean.Gillet@ulb.be, Laurence.Rongy@ulb.be, Yannick.De.Decker@ulb.be*

† Electronic supplementary information (ESI) available: Standard deviation and significance of the mean values over several simulations. See DOI: https://doi.org/10.1039/d2cp03102g

homochiral composition can be reached after a few iterations of the process in a closed batch.

A diversity of theoretical studies have been conducted in connection with enantioselective crystallisation[21–26] and Soai's asymmetric autocatalysis[5,27] but also with SMSB in the biological world.[28–31] Their objective is either to propose models that reproduce the various observations, or to highlight new mechanisms behind the emergence of homochirality. These studies typically rely on a given set of elementary processes,[4] whose dynamics can be studied with kinetic rate equations,[32] stochastic approaches[5,27,33] or population balance equations.[34,35] Using this latter method, it has been shown that chemical reactions and crystal growth might in fact obey similar dynamics.[5,25]

Models based on chemical reaction networks[4,5,36,37] are often extensions of Frank's pioneering work.[38] They often share two common ingredients: they incorporate an autocatalytic production of enantiomers from an achiral substrate, and some form of mutual antagonism between these enantiomers. This class of models can, for example, capture the behaviour of the kinetically controlled absolute asymmetric synthesis in Soai's reaction.[4,5]

SMSB in Frank-like models takes place under far-from-equilibrium conditions, which are usually obtained by controlling the concentration of the achiral reactant. In well-stirred systems, enantiomeric amplification takes place when this concentration exceeds a critical value, at which the racemic state becomes unstable. The racemic state is then replaced by non-racemic compositions through a bifurcation. These bifurcations are often symmetric, in the sense that both enantiomers are equally likely to dominate the system's composition once the bifurcation has been crossed. The final enantiomeric composition is thus fully determined by the initial chiral bias.[4,5,38–41]

New interesting behaviours can be observed when the evolution equations derived from Frank-like chemical networks are coupled with diffusion in spatially extended systems. Propagating fronts are observed in all those systems.[33,37,42–45] In a first stage, reactions govern the dynamics and local enantiomeric excesses are amplified. This results in systems composed of coexisting non-racemic domains. As diffusion proceeds, the local enantiomeric excesses slowly spread across the system and start to interact. The final stable state is either homogeneous, *i.e.* composed of a single homochiral phase, or heterogeneous (made of multiple coexisting homochiral domains).[42] In the latter case, homochirality is reached locally but from a global perspective, the average enantiomeric composition tends to be racemic for sufficiently large systems. Reaction–diffusion equations were for example used to study chiral polymerisation.[43–45] In a one-dimensional space, the final state consisted in co-existing homochiral domains while at higher dimensions, diffusion is able to create a single homochiral region very slowly. The addition of advection and turbulence has been shown to accelerate the process.[42] Similarly, local random fluctuations were shown to lead a Frank-like system either to a homochiral solution, or to the coexistence of homochiral phases.[33]

In this work, we present a novel strategy to control the dynamics of spontaneous mirror symmetry breaking in spatially extended systems. We analyse how spatial gradients of achiral reactants can affect the emergence and the propagation of homochiral domains. Using a reaction–diffusion approach, we study the properties of a Frank-like model in one-dimensional and two-dimensional systems in the presence of such gradients, to assess how breaking translational invariance affects the dynamics of enantiomeric symmetry breaking. We do not aim to provide a detailed explanation for the complex mechanisms at work in specific experiments, such as in Viedmas deracemization or Soais reaction. Our goal is rather to identify general features and parameters of importance that could be used to control the amplification of enantiomeric excess in future experiments. The article is structured as follows. Our model and the associated evolution equations are presented in Section 2. Details regarding numerical simulations are provided in Section 3. One-dimensional and two-dimensional dynamics are presented in Sections 4 and 5, respectively, and discussed in Section 6. We summarise our findings and discuss future work in Section 7.

## 2 Model and equations

To investigate the role of the achiral substrate distribution, we use a Frank-like model similar to the one proposed by Kondepudi.[39,40,46] The model can be summarised by the following chemical network, where the $k_i$ s denote the rate constants:

1. Spontaneous production:

$$2A \underset{k_{-1}}{\overset{k_1}{\rightleftharpoons}} R; \quad 2A \underset{k_{-1}}{\overset{k_1}{\rightleftharpoons}} S \tag{1}$$

2. Autocatalytic production:

$$2A + R \underset{k_{-2}}{\overset{k_2}{\rightleftharpoons}} 2R; \quad 2A + S \underset{k_{-2}}{\overset{k_2}{\rightleftharpoons}} 2S \tag{2}$$

3. System removal:

$$R + S \xrightarrow{k_s} C \tag{3}$$

The first set of reactions (1) corresponds to a spontaneous production of a chiral product from two achiral species *A*. In Kondepudi's original model, this reaction involves the production of a stereogenic center caused by the interaction between two achiral species *A* and *B*. Here, we assume that since the concentrations of *A* and *B* are maintained constant in Kondepudi's model, any distinction between these two species does not affect the dynamics of the system and we consider a single achiral species *A*. This type of reaction can be found in crystallisation processes where enantiomeric conglomerates form thanks to the association of achiral sub-units, for example in $NaClO_3$ crystals. Reactions (2) are autocatalytic productions of the two chiral species. Polymerisation or crystallisation processes present such cooperative effects.[47] Moreover, autocatalysis is also found in most processes related to the emergence of living systems.[48–51]

Autocatalysis alone is not able to lead to SMSB and a supplementary step is required. The last reaction (3) corresponds to a mutual antagonism between the enantiomers. The enantiomers react together to form an achiral product C that is

assumed to be directly removed from the system. This reaction is equivalent to a heterochiral interaction and is necessary to decrease racemicity in the system. It is the only reaction that we consider to be irreversible. Ribo *et al.* viewed the product C as an achiral heterodimer RS that can decompose into its enantiomeric precursors.[52] This reversibility was shown to slightly affect the final enantiomeric composition but not the reaction yield.

Assuming that we have an ideal system, the reaction–diffusion equations for the concentrations of species $R$ and $S$, respectively denoted as $r'$ and $s'$, read

$$\frac{\partial r'}{\partial t'} = k_1 a'^2 - k_{-1} r' + k_2 a'^2 r' - k_{-2} r'^2 - k_s r' s' + D\nabla'^2 r' \quad (4)$$

$$\frac{\partial s'}{\partial t'} = k_1 a'^2 - k_{-1} s' + k_2 a'^2 s' - k_{-2} s'^2 - k_s r' s' + D\nabla'^2 s. \quad (5)$$

In the above equations, $D$ stands for the diffusion coefficients of $R$ and $S$, which we consider to be identical and constant. Reactions (1) and (2) are seen as elementary steps in our model, so that the relation

$$\frac{k_1}{k_{-1}} = \frac{k_2}{k_{-2}} = \varepsilon \quad (6)$$

must be satisfied. The ratio $\varepsilon$ scales like the inverse of a concentration, which allows us to define non-dimensional concentrations $a = a'\varepsilon$, $r = r'\varepsilon$ and $s = s'\varepsilon$. We also introduce rescaled time units $t = t'/\tau$ with $\tau = \varepsilon^2/k_2$, and rescaled space coordinates $(x, y) = (x'/L_c, y'/L_c)$, where $L_c = \sqrt{D\tau}$. This leads to the non-dimensional evolution equations

$$\frac{\partial r}{\partial t} = \alpha a^2 - \alpha r + a^2 r - r^2 - \beta r s + \nabla^2 r \quad (7)$$

$$\frac{\partial s}{\partial t} = \alpha a^2 - \alpha s + a^2 s - s^2 - \beta r s + \nabla^2 s \quad (8)$$

where $\alpha = k_1\varepsilon/k_2$ and $\beta = k_s\varepsilon/k_2$.

In the homogeneous limit ($\nabla^2 r = \nabla^2 s = 0$), three chemically acceptable steady states ($r_s$, $s_s$) exist: two non-racemic steady states ($r_s \neq s_s$) and a single racemic steady state ($r_s = s_s$). The stability of these states is controlled by the amount of achiral compound. The system undergoes a pitchfork bifurcation, for which the critical value of the control parameter $a$ is given by:

$$a^{\text{crit}} = \sqrt{\frac{\alpha\beta + 2\alpha\sqrt{\beta} + \alpha}{\beta - 1}} \quad (9)$$

when $a < a^{\text{crit}}$, the racemic steady state is stable and no enantiomeric excess can be amplified. As soon as $a > a^{\text{crit}}$, the racemic state becomes unstable and two non-racemic branches correspond to stable steady states. This can be seen in Fig. 1, in which we plot the enantiomeric excess (EE),

$$\text{EE}\,(\%) = \left(\frac{r - s}{r + s}\right) \times 100\%, \quad (10)$$

which is a typical measure of the enantiomeric composition of a system. In this study, we consider that homochirality is reached when EE (%) $\geq$ 99.0% or EE (%) $\leq -99.0\%$.

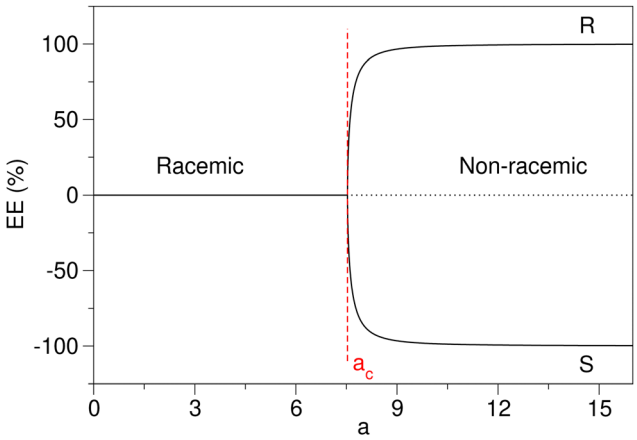


Fig. 1 Bifurcation diagram showing the homogeneous steady states of eqn (7) and (8), here expressed in terms of the enantiomeric excess, EE. Solid lines stand for stable steady states and dashed lines for unstable state. Parameters are $\alpha$ = 50, $\beta$ = 250, so that the bifurcation takes place at a critical value $a^{\text{crit}} \approx 7.53$. Note that EE (%) $\geq$ 99.0% or EE (%) $\leq -99.0\%$ are reached for concentrations larger than $a \approx 11.0$.

We observe from expression (9) that $\beta$ must necessarily be $>1$. In terms of the original parameters, this condition translates as $k_{-2} < k_s$, which is common for the type of chemical network considered here.[40,41] This condition is necessary, but not sufficient, to observe homochirality. From a chemical perspective, it means that the mutual antagonism must be predominant compared to the reverse reaction of the autocatalytic production of enantiomers.

## 3 Numerical simulations

Eqn (7) and (8) were numerically integrated with a fourth-order Runge–Kutta scheme and finite differences were used for spatial discretisation. One-dimensional and two-dimensional systems were investigated. For the latter, we used a square system such that the length $L_x$ and the width $L_y$ are equal ($L_x = L_y = L$). In both cases, we imposed no-flux boundary conditions for the concentrations $r$ and $s$ at all boundaries. The initial conditions for $r$ and $s$ in each cell were independently sampled from a Gaussian distribution centered on a prescribed value $r_0^d$ and $s_0^d$, respectively, such that $r_0^d = s_0^d$ and whose standard deviation was $r_0^d/100$ ($s_0^d/100$). Such initial conditions are equivalent to a globally racemic mixture with local fluctuations. The global EE was always close or equal to 0, despite local fluctuations. We consider that this scenario of a fluctuating local enantiomeric composition is more likely to be representative of reality, since a homogeneous enantiomeric excess across a macroscopic system is highly improbable, as suggested by Hochberg and Zorzano.[33] More generally, perfect racemic mixing is very unlikely if not impossible for any finite-size molecular system.

The solutions of eqn (7) and (8) were found to converge upon decreasing the temporal ($dt$) and spatial ($dx$, $dy$) step sizes. Typical values that were used are $dt = 5.0 \times 10^{-8}$ and $dx = dy = 5.0 \times 10^{-4}$. Inspired by Kondepudi's original work, we chose to

 

work with $\alpha = 50$ and $\beta = 250$. Such values provide enantiomeric amplification within reasonable time scales and correspond to a critical value $a^{crit} \approx 7.5$. In most cases, concentration values for $a$ were chosen such that the system is far beyond this bifurcation point. The initial concentrations are such that $1.0 < r^d < 10.0$ ($1.0 < s^d < 10.0$). No significant influence on the dynamics is observed in this range of values.

# 4 One-dimensional systems

## 4.1 Homogeneous achiral reactant concentration

Numerical integrations using homogeneous initial conditions for the concentration $r$ and $s$ and a homogeneous distribution of $a$ lead to the same results as in the well-stirred limit: the steady state is homogeneous and fully determined by the initial enantiomeric excess and the value of $a$. However, when fluctuating initial conditions are introduced, multiple profiles can be obtained, as shown in Fig. 2. We discuss the properties of these profiles below.

**4.1.1 Spatial profiles.** The graphs in Fig. 2 correspond to typical profiles obtained for relatively long times. These profiles are still subject to very slow temporal variations but the overall profile shape does not change anymore, as already pointed out in previous works.[42] We can, thus, safely assume that the profiles seen in Fig. 2 qualitatively correspond to the asymptotic solutions.

These profiles are consistent with those found in the literature[33,37,42–45] and illustrate the two types of situations that can be observed: (i) a homogeneous state where the EE is constant in space (Fig. 2a), or (ii) a heterogeneous steady state characterised by the coexistence of multiple homochiral domains (Fig. 2b–d). Some initial conditions thus lead to globally homochiral systems, while others give rise to local homochirality. Only global homochirality can lead to an average EE that is $\geq 99\%$ or $\leq -99\%$. Note that in the remainder of this study, the random initial conditions (IC) associated to the steady profiles (a) and (b) (Fig. 2a and b), for $L = 0.5$, will be denoted as IC I and IC II, respectively. These initial conditions will be reused to investigate the influence of the different parameters of interest on the final enantiomeric composition.

**4.1.2 Global homochirality.** Because of the stochastic character of the initial conditions, isolated numerical simulations such as those presented in Fig. 2 do not allow to draw general conclusions on the role played by the model's parameters on the probability to reach global homochirality. We thus performed multiple simulations starting from different fluctuating initial conditions, and computed this probability at different concentrations of the achiral reactant $a$, and at different sizes $L$. The resulting statistics are reported in Fig. 3.

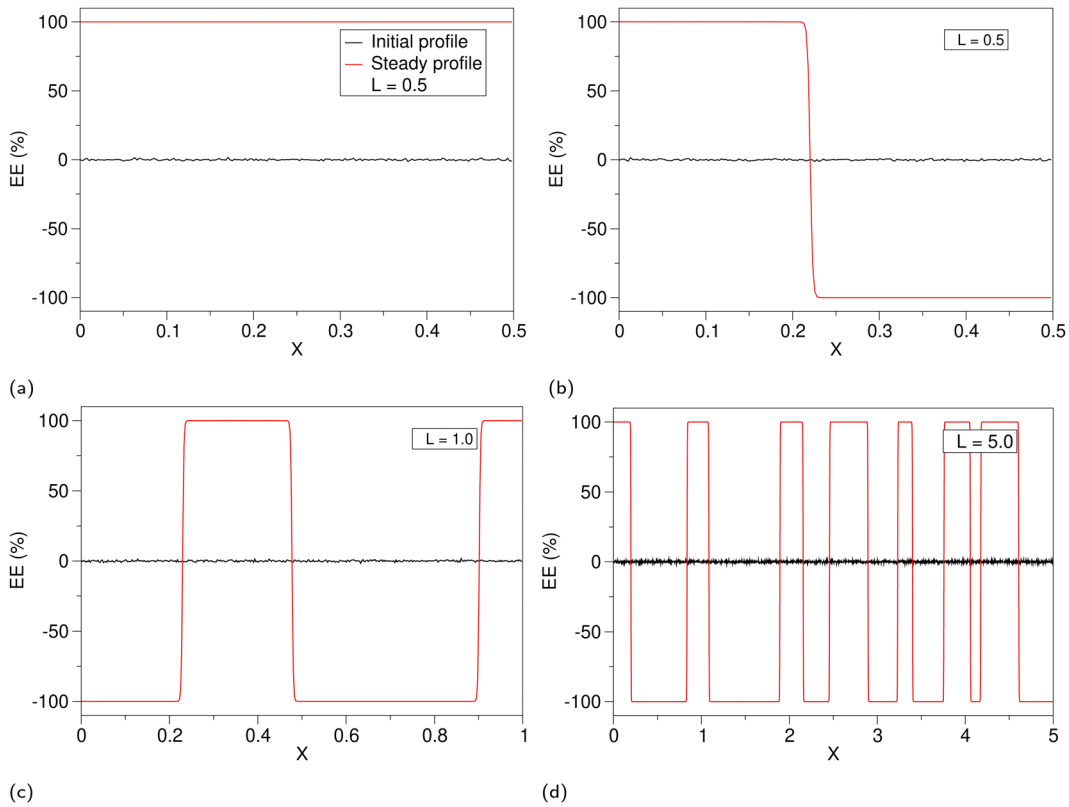


Fig. 2 Illustration of various steady profiles obtained for different system sizes: (a and b) $L = 0.5$, (c) $L = 1.0$, (d) $L = 5.0$. Solid black lines represent the randomly generated initial distributions of the enantiomeric excess whereas solid red lines stand for the steady distributions. Profile (a) is characterised by a homogeneous steady profile whereas profiles (b–d) are heterogeneous profiles. The initial profiles from (a and b) are respectively denoted as IC I and IC II. The steady profiles are obtained after a total simulation time $t_{tot} = 0.2$ and the parameters are: $a = 75.0$, $r_0^d = 10.0$, $s_0^d = 10.0$.

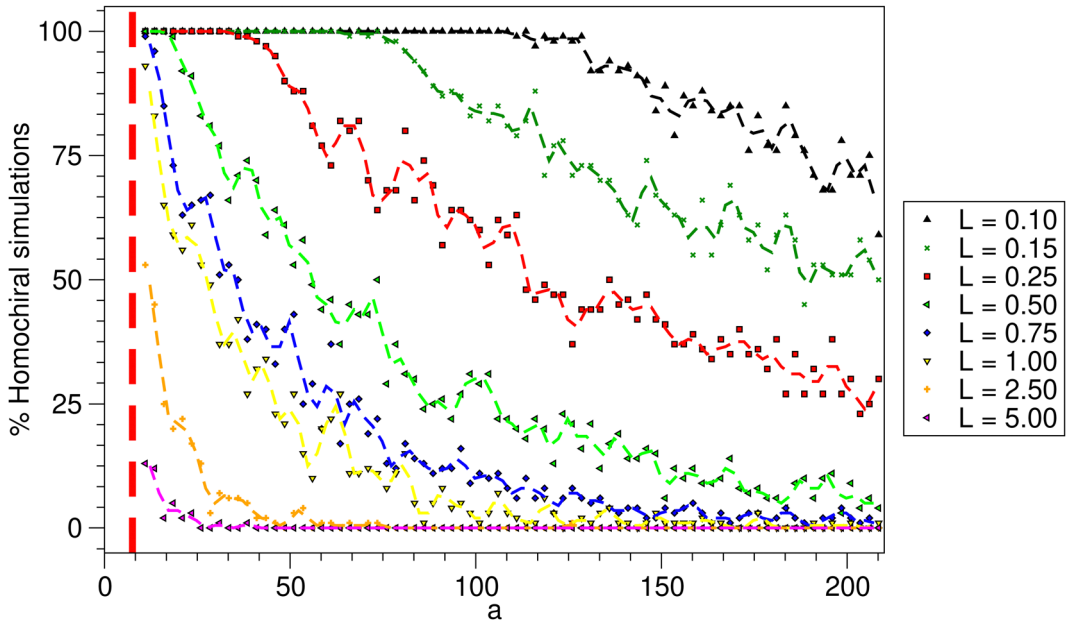


Fig. 3 Evolution of the percentage of simulations exhibiting homochirality as a function of the control parameter $a$ at various system sizes $L$, increasing from right to left. Each point is calculated from 100 simulations. The vertical red dashed line corresponds to the critical value $a^{crit}$ and the other lines are guides for the eye. Simulation parameters: $t_{tot}$ = 0.5, $r_0^d$ = 1.0, $s_0^d$ = 1.0.

First, we recall that in the homogeneous limit with no diffusion, a homochiral composition is observed when $a > a^{crit}$ (*cf.* eqn (9)). In the presence of diffusion and local initial inhomogeneities, we observe that the greatest probability to obtain a homogeneous homochiral composition is reached near the bifurcation point. This probability decreases with increasing values of the control parameter $a$ and tends to zero for large values of this parameter. Second, we see that for a given concentration $a$, the system size dramatically influences the percentage of simulations resulting in global homochirality. The probability to observe a final homogeneous homochiral state decreases as the size $L$ increases. This can be directly correlated with the increasing probability to have a greater number of domains when the system size is large, as can already be seen in Fig. 2.

We can conclude from these trends that the achiral reactant plays an ambivalent role in the emergence of homochirality in a spatially extended system: a certain amount is required to witness homochirality, but excessive quantities reduce the chance of obtaining global homochirality because of the coexistence of domains of opposite handedness.

**4.1.3 Time scales.** The average time required to reach homogeneous final states, when observed, is calculated from the fraction of simulations that ended in global homochirality and is plotted in Fig. 4 as a function of the achiral reactant concentration for three system sizes. We remind that we keep $a > a_{crit}$. We observe that the average times are typically larger for larger systems. The three curves exhibit a minimum, suggesting once more an ambiguous role of $a$. Insufficient or excessive amounts of achiral reactant delay the emergence of a single homogeneous homochiral state.

As we will discuss later, the achiral reagent concentration affects the mechanisms of local enantiomeric excess amplification, thereby influencing the probability of observing global homochirality as well as time scales.

### 4.2 Concentration gradient of achiral reactant

We now impose a time-independent constant gradient of $a$ in the system:

$$a(x) = a_0 + (a_L - a_0)\frac{x}{L}, \tag{11}$$

where $a_0 = a(0)$ and $a_L = a(L)$. The presence of this profile modifies the structure of the model, even in the limit where $r$ and $s$ are homogeneously distributed in the system.

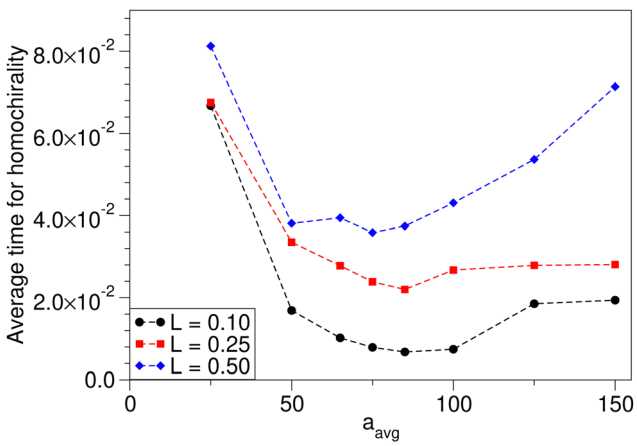


Fig. 4 Average time required to reach global homochirality as a function of the concentration of achiral reactant. The achiral reactant is homogeneously distributed. The average time is derived from the fraction of simulations in Fig. 3 that resulted in global homochirality. Dashed lines are only visual aids. Simulation parameters: $r_0^d$ = 1.0, $s_0^d$ = 1.0.

 

Considering $\nabla^2 r = \nabla^2 s = 0$ in eqn (7) and (8), integrating over $x$ and dividing by $L$ leads to

$$\frac{dr}{dt} = (\alpha + r)\delta - \alpha r - r^2 - \beta rs \quad (12)$$

$$\frac{ds}{dt} = (\alpha + s)\delta - \alpha s - s^2 - \beta rs, \quad (13)$$

introducing a new parameter

$$\delta = \frac{1}{3}(a_L{}^2 + a_L a_0 + a_0{}^2). \quad (14)$$

$\delta$ depends on the boundary conditions $a_0$ and $a_L$ and plays the same role as $a^2$ in the homogeneous limit of eqn (7) and (8). We can thus conclude that the concentrations of $A$ at the boundaries can be used as control parameters, since beyond a certain critical value of $\delta$ corresponding to a pitchfork bifurcation, the stable racemic composition becomes unstable and the system evolves towards two possible non-racemic steady states. The structure of eqn (12) and (13) being similar to that of eqn (7) and (8) with $\delta$ playing the role of $a^2$, the critical value of $\delta$ can be directly derived from relations (9) and (14). Given the form of $\delta$, multiple combinations of $a_0$ and $a_L$ can lead to SMSB, as long as the condition $\delta^{crit} \geq (a^{crit})^2$ is fullfilled.

**4.2.1 Spatial profiles.** We now turn to the properties of spatially-extended systems. We first note that in contrast to the case of homogeneously distributed $a$, simulations carried out with a linear profile of $a$ systematically lead to global homochirality, for all (fluctuating) initial conditions tested. An example of the dynamics leading to such homochirality is given in Fig. 5, for a system starting with initial condition IC II.

Local homochirality quickly appears on the right side of the system, where the concentration $a$ is the largest. This results in the rapid appearance of two homochiral domains of opposite handedness, in a way similar to what can be seen for systems with homogeneous distributions of $A$ (see Fig. 2b). In the present case, however, the coexistence of several domains is not a stable situation. As time goes by, the domain which is closest to the maximum value $a_{max} = a_L$ (here the $R$-rich domain with an EE of almost 100%) expands and invades the domain of opposite chirality. The final result is the complete disappearance of the $S$-rich domain and the formation of a single homogeneous domain, which corresponds to global homochirality.

To better understand how an inhomogeneous profile of $a$ can lead to such effects, we study the dynamics of an anti-symmetric initial condition where two equal domains of opposite handedness coexist (see Fig. 6a and b). We compare the system's response for profiles of $a$ of opposite slopes. One can see that the domain in which the concentration of $a$ is larger always invades the other one, which can result in homochiral system whose EE is close to ±100%, depending on the sign of the slope.

The evolution of the concentration profiles are shown in Fig. 6c and d for a positive gradient of $a$. In that case, the concentration of enantiomer $S$ increases everywhere by reaction and diffusion, leading to a final stable state dominated by this enantiomer whose local concentration depends on the local

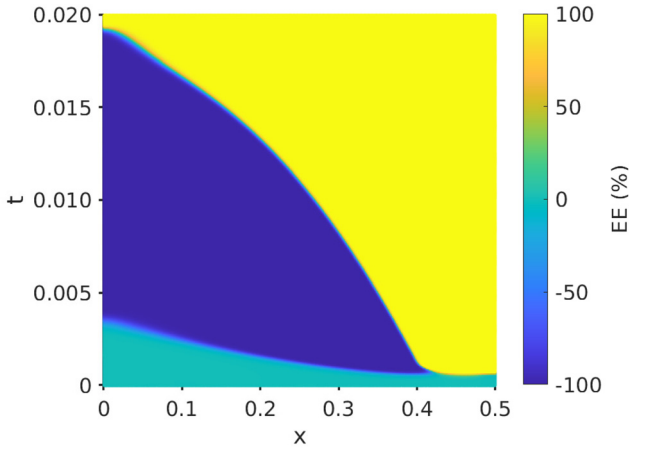


Fig. 5 Space-time plot of the enantiomeric excess, starting from IC II with a fixed concentration gradient of achiral substrate concentration $a$. Simulation parameters: $t_{tot} = 0.02$, $L = 0.5$, $a_0 = 0$, $a_L = 150$, $r_0^d = 10.0$, $s_0^d = 10.0$.

value of $a$. Because $a$ controls the rate of production of enantiomers, the $S$-rich region produces $S$ more rapidly than the $R$-rich region produces $R$ and therefore invades the $R$-rich region by diffusion. A similar argument holds in reverse when the slope of $a$ changes sign.

**4.2.2 Time scales.** A linear profile of $a$ qualitatively affects the properties of the model in the sense that it allows for systematic global homochirality. In this Section, we analyse how such a profile affects the time needed to reach global homochirality.

To compare different profiles, we introduce the slope $p = (a_L - a_0)/a_L$). Fig. 7a compares the average time required to attain global homochirality for linear profiles of $a$ with different slopes $p \neq 0$, for the same system size $L = 0.10$. We note that when $A$ is inhomogeneously distributed, minima are also observed but appear to be shifted with increasing average values of $a$, defined as $a_{avg} = 1L\int a(x)dx$. This situation is thus similar to what is observed for constant $a$ ($p = 0$), where the average time is also minimum for a given value of $a_{avg}$, denoted as $a_{avg}^{min,p=0}$. We notice that, when $a_{avg} < 100$, the higher the slope, the lower the average time at a given $a_{avg}$. On the other hand, when $a_{avg} \geq 100$ and $a_{avg} > a_{avg}^{min,p}$, the trend is reversed and the effect of $a_{avg}$ on the average time is stronger. We witness once more a variable role of the precursor concentration $a$.

A similar trend is observed for the average enantiomer production rate. We define this quantity as the average enantiomer concentration at the steady state, divided by the average time required to obtain it. We observe in Fig. 7b that the production rate increases with $a_{avg}$. When $a_{avg} < 160$, the highest rates are obtained with the steepest profiles ($p = 100\%$). This effect is reversed for $a_{avg} > 160$ where the profile $p = 75\%$ provides the highest production rate for high value of $a_{avg} > 300$. Regardless of the value of $p$, the production rate does not change significantly beyond $a_{avg} = 100$. From these observations, it appears that the concentration gradients always offer high production rates since the final state is systematically homochiral. These rates can be maximised by choosing the optimal combination of $a_{avg}$ and $p$.

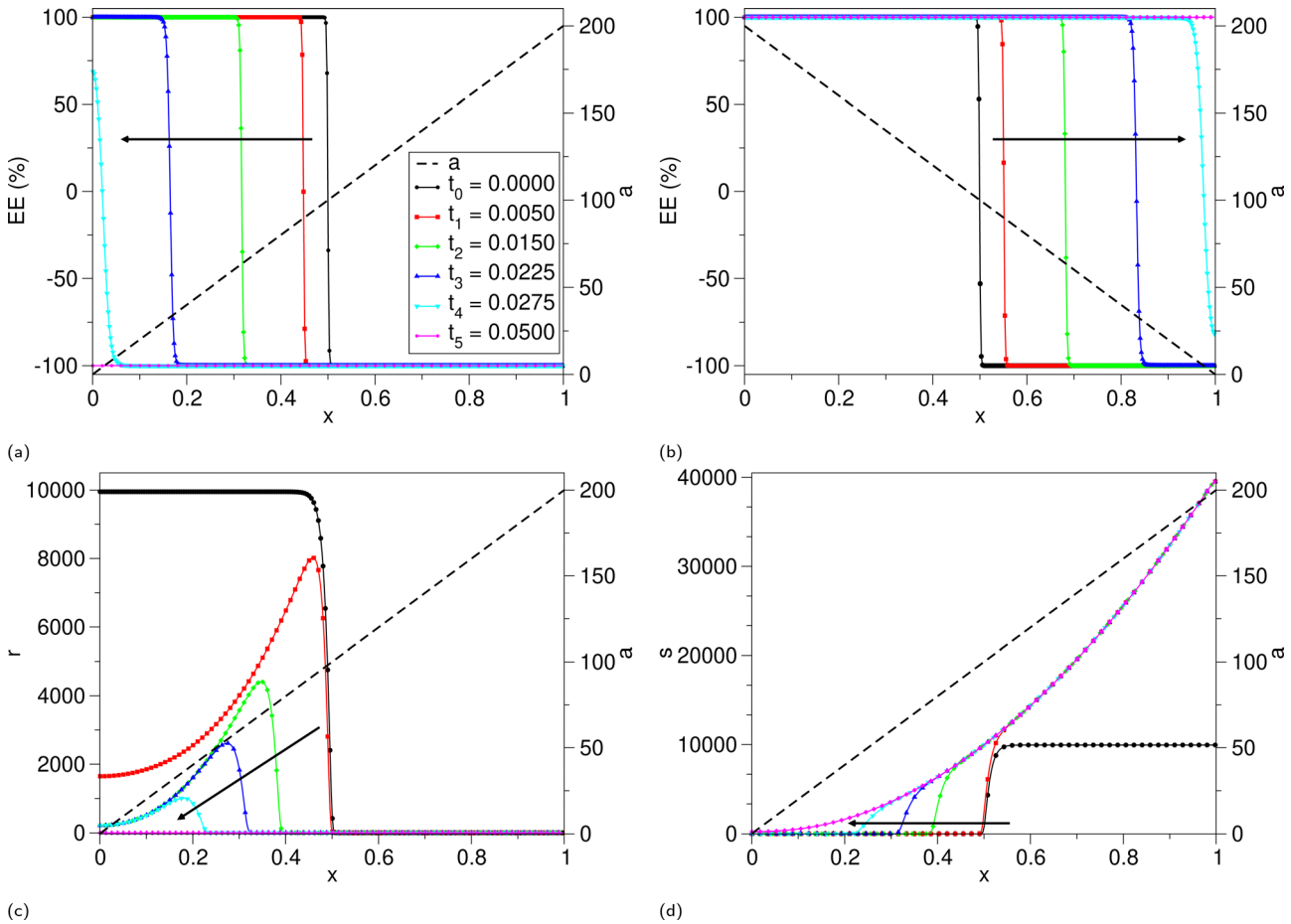


Fig. 6 Effect of linear profiles of $a$ of opposite slopes on a stable antisymmetric initial configuration composed of two equal homochiral domains of equal size. Evolution of EE as a function of time for (a) $a_0 = 0$, $a_L = 200$; (b) $a_0 = 200$, $a_L = 0$. Evolution of the concentration profiles of $r$ (c) and $s$ (d) when $a_0 = 0$ and $a_L = 200$. The responses are shown at different times. The arrows indicate increasing time.

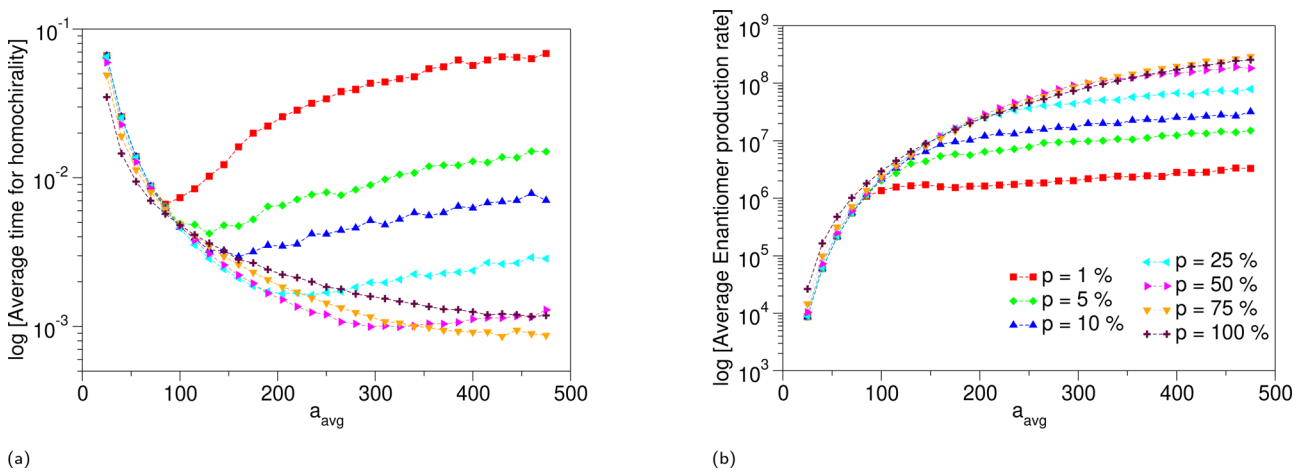


Fig. 7 Evolution of (a) the time required to reach global homochirality and (b) the enantiomer production rate as a function of the average concentration of achiral reactant. Each point is obtained from a sample of five hundred simulations. The results with error bars representing the standard deviation are given in the ESI.† The various colours are associated to the various slopes intensities according to the parameter $p$. Dashed lines are guides to the eye. Simulation parameters: $r_0^d = 1.0$, $s_0^d = 1.0$, $L = 0.1$.

 

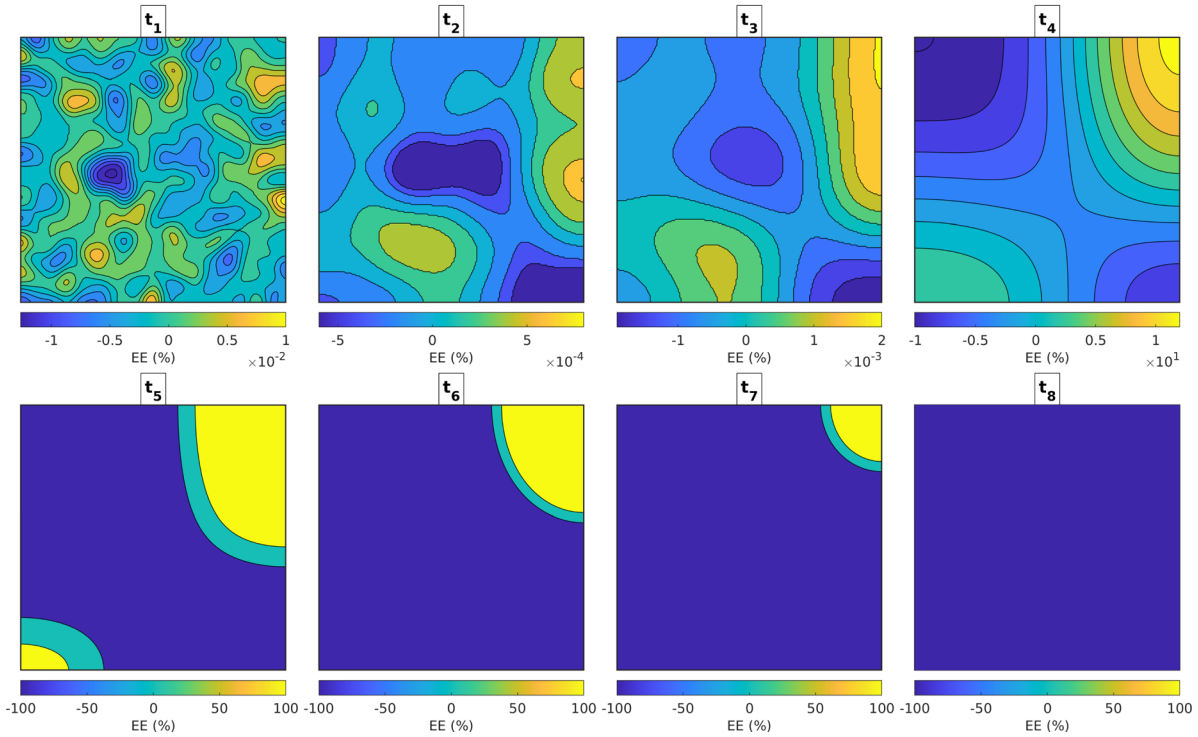


Fig. 8 Evolution of the EE profiles at different times in a two-dimensional system, starting from fluctuating initial conditions with a homogeneous concentration of achiral substrate concentration $a$. Simulation parameters: $t_1 = 6.00 \times 10^{-3}$, $t_2 = 6.00 \times 10^{-2}$, $t_3 = 1.50 \times 10^{-1}$, $t_4 = 6.00 \times 10^{-1}$, $t_5 = 9.00 \times 10^{-1}$, $t_6 = 1.50$, $t_7 = 1.95$, $t_8 = 2.40$, $L = 0.10$, $a = 150$, $r_0^d = 1.0$, $s_0^d = 1.0$.

To summarise, imposing inhomogeneous profiles of the achiral reactant A confirms the ambivalent role played by this species in 1-dimensional systems. The biggest advantage is the suppression of the coexistence of homochiral domains. The use of the gradient therefore opens the way to homogeneous homochiral states which can be obtained on improvable time scales, by controlling the average concentration of achiral species and its spatial distribution. We now turn to the case of 2-dimensional systems.

## 5 Two-dimensional systems

In one-dimensional systems, homogeneous homochirality is not systematically obtained and homochiral domains can coexist. It is no longer the case with an additional dimension and homochiral domains are not able to coexist anymore. Numerical integrations in 2D using fluctuating initial conditions and a homogeneous distribution of $a$ were first performed. An example of observed dynamics is featured in Fig. 8 where the distribution of the enantiomeric excess in space is shown at different times. First, small-scale domains merge to form larger regions. As time goes by, these regions evolve into homochiral regions. After a certain time, a large $S$-region covers the majority of the system, surrounding two smaller $R$-domains, and progressively invades these domains to ultimately result in a homogeneous homochiral state $S$, in this case. The disappearance of coexistence is primarily due to curvature effects in the propagation front, which are ubiquitous in two-dimensional systems. The homochiral domains in contact will compete with each other and because the inner front is shorter than the outer one, the interface separating them propagates in the direction of the curvature.[42] Systematic global homochirality is also observed when numerical simulations are performed using a concentration gradient of achiral reactant parallel to the $x$ axis such that:

$$a(x, y) = a_0 + (a_L - a_0)\frac{x}{L}, \quad (15)$$

where $a_0 = a(0,y)$ and $a_L = a(L,y)$.‡ Thus, we can conclude that homochirality is just a matter of time in 2D, whether using homogeneous or linear concentrations profiles of $a$. In Fig. 9a, the mean time required to reach global homochirality is plotted as a function of the average concentration of achiral reactant. When the average concentration of achiral reactant remains at relatively low levels ($a_{avg} < 65$), the average time decreases when increasing $a_{avg}$ but the effect of $p$ is negligible. Minima are observed regardless of the value of $p$, as in 1D (*cf.* Fig. 7a). This highlights again the ambivalent role played by the achiral reactant concentration. As observed in 1D, past a certain threshold, the time scales for global homochirality increase with $a_{avg}$ and when $p$ becomes higher (in 2D, $a_{avg} > 65$).

To better measure this apparently counterproductive effect, the production rate of enantiomers is plotted as a function of the average concentration in Fig. 9b. Optima of production are observed for each value of $p$ but the concentration gradients are

‡ Considering the limit where $r$ and $s$ are homogeneously distributed in the system, such profiles provide the same equations as eqn (12) and (13).

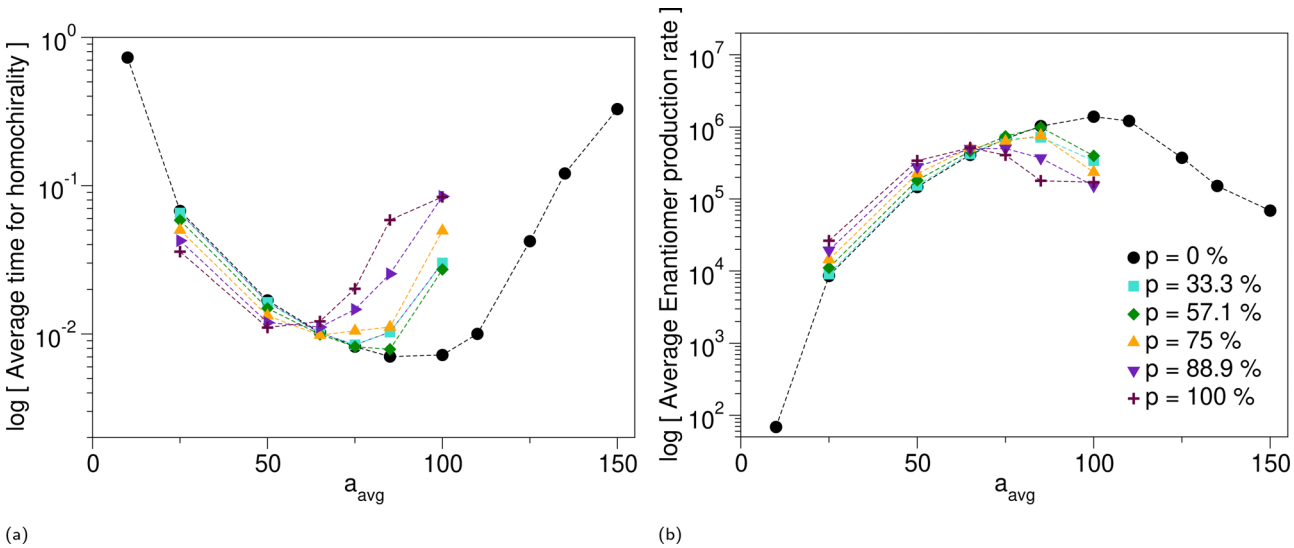


Fig. 9 Two-dimensional results. Evolution of (a) the time required to reach global homochirality and (b) the enantiomer production rate as a function of the average concentration of achiral reactant. Each point is obtained from a sample of 100 simulations. The various colours are associated to the various slopes intensities according to the parameter $p$. Simulation parameters: $r_0^d = 1.0$, $s_0^d = 1.0$, $L = 0.1$.

Table 1 Achiral reactant concentration profiles maximising the productions rates in two-dimensional systems

| $a_{avg}$ | $p$ (%) | Production rate |
|---|---|---|
| 25 | 100 | $2.63 \times 10^4$ |
| 50 | 100 | $3.41 \times 10^5$ |
| 65 | 100 | $5.14 \times 10^5$ |
| 75 | 57.1 | $7.43 \times 10^5$ |
| 85 | 0 | $1.03 \times 10^6$ |
| 100 | 0 | $1.39 \times 10^6$ |

more efficient at low average concentrations ($a_{avg} \leq 65$). In other words, if the amount of achiral reactant is limited, it seems preferable to distribute it using linear profiles. However, the efficiency gain is minimal. If concentration is further increased, the uniform distribution is more efficient. The maximum production rate is obtained using a homogeneous profile of the achiral reactant at $a_{avg} = 100$ (see Table 1).

# 6 Discussion

Results from the previous two sections have repeatedly highlighted an ambivalent role of the achiral reactant. Even if the effect of the concentration $a$ is not trivial, 1D and 2D results suggest that the same mechanism is involved.

## 6.1 Homogeneous achiral reactant concentration

Diffusion is a slow process and needs time to settle. In the early stages, the local enantiomeric excesses are rapidly amplified. The amount of enantiomers produced in each spatial element is limited by the achiral reactant concentration. Adjacent cells that share the same dominant enantiomer will merge to form domains, otherwise they will compete for dominance. In 1D systems, the ultimate result can therefore be co-existing homochiral domains of opposite handedness (Fig. 2).

When $a$ is sufficiently low, the concentrations $r$ and $s$ remain at a relatively low level in the early stages. This leaves the opportunity for diffusion to homogenise more easily the initial local enantiomeric excesses and allow the system to ultimately reach global homochirality. However, the characteristic diffusion time $t_c$ depends upon the size of the system as $t_c \sim L^2/D$, which explains the influence of the system size on the dynamics observed in 1D (Fig. 3).

As $a$ increases, higher level of concentrations $r$ and $s$ are reached after a few iterations. This more efficient amplification reduces the time window for the homogenisation process to take place. A direct consequence is that initial inhomogeneities are more likely to remain and be amplified. When homochiral domains are formed and come in contact, diffusion is not able to homogenise the system due to the "System removal" reaction (eqn (3)). As soon as enantiomers are transported in a neighbour domain of opposite handedness, these are directly eliminated by the opposite enantiomer due to the 1–1 stoichiometry of the reaction. The fraction of dominating enantiomer is quickly regenerated thanks to an inexhaustible source of achiral reactant. Hence, multiple stable homochiral domains can emerge from the initial heterogeneous distribution of EE. In 1D, the absence of inhomogeneities in the distribution of $a$ guarantees equal steady concentration levels in each cell and thus, stability of the domains (Fig. 2). In 2D, the coexistence of domains cannot persist in the long term due to curvature effects. Unless a perfectly straight interface is formed between two homochiral domains, curvature effects will always favour the progressive propagation of a domain at the expense of others, which ultimately results in global homochirality (Fig. 8).

This effect of $a$ on the amplification of initial local enantiomeric excess can also explain the presence of a minimum in the curves for the time needed to reach homochirality in 1D and 2D as a function of $a$ (Fig. 4 and $p = 0$ in Fig. 9a). An increase of its

 

value accelerates the overall dynamics. However, when local concentrations exceed a certain value, the amplification process becomes too rapid and the initial inhomogeneities are amplified rather than being homogenised. Thus, more homochiral regions are susceptible to emerge and coexist for longer time, delaying thereby the eventual global homogenisation.

The position of the minima can be evaluated by comparing the diffusive and kinetic time scales, respectively denoted $\tau'_{\mathrm{diff}}$ and $\tau'_{\mathrm{kin}}$. By assuming that the scales of these competing processes are equal, $\tau'_{\mathrm{kin}} = \tau'_{\mathrm{diff}}$ at the minimum, we can estimate the value of $a$ where the homogenisation process and the amplification process are balanced. We consider $\tau'_{\mathrm{kin}}$ to be primarily governed by autocatalytic production reactions such that $\tau'_{\mathrm{kin}} = 1/k_2 a'^2$. On the other hand, the diffusive time scale must depend on a certain length but it seems unlikely that it is sensitive to the total size of the system (see Fig. 4, where the length of the system does not influence the position of the minimum significantly). Therefore, we make the hypothesis that there exists a certain typical length, $l'_{\mathrm{H}}$ associated with the process of homogenisation of the initial enantiomeric excesses.

The diffusive time scale is thus given by $\tau'_{\mathrm{diff}} = l'^2_{\mathrm{H}}/D$. The conversion of kinetic and diffusive time scales to dimensionless quantities gives, for the position of the minimum,

$$a^{\min} = \frac{1}{l_{\mathrm{H}}}. \tag{16}$$

Although we have no exact value for $l_{\mathrm{H}}$, we suggest that this length might be related to the interaction between enantiomer production reaction (eqn (1)) and mutual antagonism (eqn (3)). Based on those time scales, we can construct a diffusive length scale $l_{\mathrm{h}'} = \sqrt{D\tau_1}$, with $\tau_1 = \varepsilon/k_1$ or $l'_{\mathrm{H}} = \sqrt{D\tau_{\mathrm{s}}}$ with $\tau_{\mathrm{s}} = \varepsilon/k_{\mathrm{s}}$. The former gives $l'_{\mathrm{H}} = 1/\sqrt{\alpha}$ and the latter $l_{\mathrm{h}} = 1/\sqrt{\beta}$. Replacing in eqn (16), we obtain an $a_{\min}$ value comprised between (7) and (16). Such values provide a first approximation of the same order of magnitude as the values of the minima observed in 1D or 2D (Fig. 4 and 9).

### 6.2 Concentration gradient of achiral reactant

The presence of a linear profile of achiral reactant was shown to suppress any possible coexistence in 1D. The combination of an inhomogeneous distribution of $a$ and its continuous supply contributes to the destabilisation of interfaces between homochiral domains. The early-time homochiral region that benefits from the highest local concentration $a$ will grow, propagate, and invade the whole system. The result is a single final homochiral state. The introduction of the concentration gradient helps to better understand that establishing a homogeneous homochiral profile is a two-step process, as illustrated in Fig. 10. At first, the local enantiomeric excesses are rapidly amplified and homochiral domains appear throughout the system, depending on the local fluctuations. This process is governed by the local kinetics of the system. Then, as amplification proceeds, a slower diffusion-controlled regime takes over. Consequently, the time evolution of the global EE consists of two stages, a reaction-controlled one and a diffusion-controlled one as shown in Fig. 10, where we compare the evolution of the average EE in time with or without diffusion of the two enantiomers.

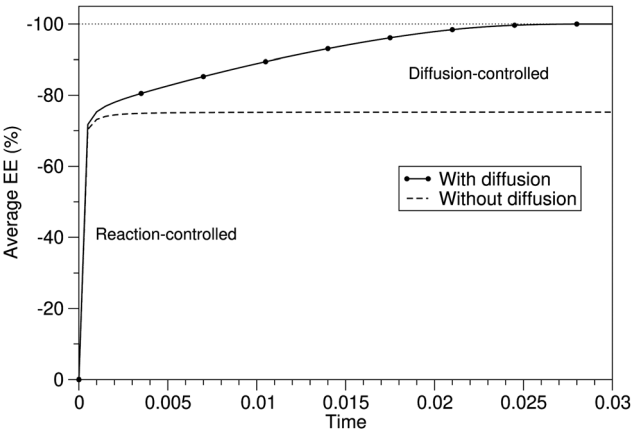


Fig. 10 Illustration of the effect of diffusion processes on the evolution in time of the average enantiomeric excess. Simulation parameters: $t_{\mathrm{tot}} = 0.1$, $a_0 = 0$, $a_{\mathrm{L}} = 200$, $r_0^{\mathrm{d}} = 10.0$, $s_0^{\mathrm{d}} = 10.0$, $L = 1.0$.

Minima are observed for the time needed to reach global homochirality regardless of the value of the slope $p$. However, linear profiles with increasing values of $a_{\mathrm{avg}}$ monotonously increase the production rate of enantiomers in 1D (Fig. 7), while in 2D maxima are observed in the production rate for all values of the slope $p$ (Fig. 9). Furthermore, the slope has a variable effect on the time scales depending on $a_{\mathrm{avg}}$. As long as $a_{\mathrm{avg}} < 100$ in 1D or $a_{\mathrm{avg}} < 65$ in 2D, $p$ does not have a significant effect. On the other hand, when $a_{\mathrm{avg}} > 100$ in 1D, larger $p$ values are better whereas in 2D, when $a_{\mathrm{avg}} > 65$, a slope $p = 0$ offers the smallest time scales possible.

To understand such results, we must remember that high local concentrations can either be reached using uniform or linear concentrations profiles. However, for a given value $a_{\mathrm{avg}}$, linear profiles will automatically imply higher local concentration levels than uniform profiles. Thus, an excessive increase of $a(x)$ through increasingly intense gradients allows the inhomogeneties to subsist longer, which slows down the evolution to a final homogeneous homochiral state. This explains the mixed role of the slope $p$ at 1D and 2D, as well as the shifts in the minima observed for time scales (Fig. 9a). A compromise must therefore be found for the way in which the precursor is distributed. Once more, the interplay between inhomogeneities and achiral reactant concentration appears crucial.

## 7 Conclusion

Spontaneous mirror symmetry breaking (SMSB) is one of the most curious features observed in both nature and experimental systems. Numerous theoretical works have been conducted in order to understand the general underlying mechanisms or to explore new systems where SMSB can be induced and controlled.[4,5,47,53] Chemical models exhibiting homochirality have been constructed since the 50s. At that

time, Frank proposed a description of a minimal system containing all the necessary ingredients to observe SMSB.[38] This model has been extensively studied and used as a basis for the construction of more complex models.[5,36,37,47] In particular, the behaviour in space of Frank-like models have been studied using various approaches. Our work aims to complete the studies where reaction–diffusion equations were solved for models exhibiting homochirality.[42–44]

In this study, we have shown that inhomogeneities in the initial distribution of enantiomers can have a tremendous influence on the behaviour of a Frank-like model undergoing reaction–diffusion processes. A direct consequence is that the achiral precursor can play an ambivalent role.

In one dimension, simulations do not systematically reach global homochirality. Various steady profiles of enantiomeric excesses (EE) and concentrations can be obtained, resulting either in homogeneous or heterogeneous homochirality, where multiple mirror homochiral domains co-exist, as already pointed out in literature.[42] In addition to this observation, we have shown the strong dependence of the final enantiomeric composition on the achiral reactant concentration and on the system size. We have also shown that systematic global homochirality can be restored when constant concentration gradients of achiral reactant are introduced. However, no control on the final spatial distribution of the enantiomeric composition appears to be possible.

In two dimensions, homochiral domains do not longer coexist and global homochirality is always reached. The situation changes due to the presence of curvature effects. Unless a perfectly straight interface is formed between two homochiral domains, curvature effects will always favour the propagation of a domain at the expense of others, which ultimately results in global homochirality. However, the time needed to reach homochirality can dramatically be influenced by the concentration of achiral reactant. Insufficient or excessive concentrations turn out to be counter-productive. This is also true when we consider the amount of enantiomer produced. Once more, we have a demonstration of the ambivalent influence of the achiral reactant concentration on the dynamics of SMSB.

Through these different results, we have highlighted the importance of the spatial distribution of the achiral reactant and the initial enantiomeric excess during SMSB in reaction–diffusion systems. Parallels can be drawn with some experimental results regarding SMSB. Steendam *et al.* have performed the synthesis of an enantiopure compound from achiral material by combining a reversible organic reaction with Viedma ripening.[54] It has been shown that increasing concentrations of achiral precursor can slow down the SMSB process. They suggested that at low concentration of achiral reactant, fewer crystals have to be deracemised and deracemisation thus proceeds faster. Our work does not claim to explain such results but provides insights regarding some observed features. For instance, the data on the various optima of achiral reactant concentration regarding the enantiomer production rate might guide future experimental works.

At this point, the achiral reactant has been considered constant in time. Future works will investigate the effect of variable achiral reactant concentration on SMSB in spatially extended systems. Moreover, we have assumed that both enantiomers diffuse at the same rate but recent experimental reports on chirality differentiation[55–57] by diffusion might challenge this assumption, which we will investigate in a subsequent work.

## Conflicts of interest

There are no conflicts to declare.

## Acknowledgements

The authors thank the Fonds de la Recherche Scientifique - FNRS for the financial support. Jean Gillet is a FRIA grantee of the Fonds de la Recherche Scientifique - FNRS.

## References

1 L. Pasteur, *C. R. Hebd. Seances Acad. Sci., Ser. D*, 1848, **26**, 535–539.
2 Q. Sallembien, L. Bouteiller, J. Crassous and M. Raynal, *Chem. Soc. Rev.*, 2022, **51**, 3436–3476.
3 W. A. Bonner, *Origins Life Evol. Biospheres*, 1991, **21**, 59–111.
4 T. Buhse, J.-M. Cruz, M. E. Noble-Terán, D. Hochberg, J. M. Ribó, J. Crusats and J.-C. Micheau, *Chem. Rev.*, 2021, **121**, 2147–2229.
5 Y. Saito and H. Hyuga, *Rev. Mod. Phys.*, 2013, **85**, 603–621.
6 D. G. Blackmond, *Chem. Rev.*, 2020, **120**, 4831–4847.
7 J. Gillet, *Chim. Nouv.*, 2021, **137**, 1–10.
8 D. K. Kondepudi, R. J. Kaufman and N. Singh, *Science*, 1990, **250**, 975–976.
9 C. Viedma, *Phys. Rev. Lett.*, 2005, **94**, 065504.
10 W. L. Noorduin, B. Kaptein, H. Meekes, W. J. P. van Enckevort, R. M. Kellogg and E. Vlieg, *Angew. Chem., Int. Ed.*, 2009, **48**, 4581–4583.
11 R. R. E. Steendam, M. C. T. Brouwer, E. M. E. Huijs, M. W. Kulka, H. Meekes, W. J. P. van Enckevort, J. Raap, F. P. J. T. Rutjes and E. Vlieg, *Chem. – Eur. J.*, 2014, **20**, 13527–13530.
12 C. Viedma, J. E. Ortiz, T. de Torres, T. Izumi and D. G. Blackmond, *J. Am. Chem. Soc.*, 2008, **130**, 15274–15275.
13 L.-C. Sögütoglu, R. R. E. Steendam, H. Meekes, E. Vlieg and F. P. J. T. Rutjes, *Chem. Soc. Rev.*, 2015, **44**, 6723–6732.
14 M. W. van der Meijden, M. Leeman, E. Gelens, W. L. Noorduin, H. Meekes, W. J. P. van Enckevort, B. Kaptein, E. Vlieg and R. M. Kellogg, *Org. Process Res. Dev.*, 2009, **13**, 1195–1198.
15 W. L. Noorduin, E. Vlieg, R. M. Kellogg and B. Kaptein, *Angew. Chem., Int. Ed.*, 2009, **48**, 9600–9606.
16 S. B. Tsogoeva, S. Wei, M. Freund and M. Mauksch, *Angew. Chem., Int. Ed.*, 2009, **48**, 590–594.
17 A. M. Flock, C. M. M. Reucher and C. Bolm, *Chem. – Eur. J.*, 2010, **16**, 3918–3921.

 

18 D. T. McLaughlin, T. P. T. Nguyen, L. Mengnjo, C. Bian, Y. H. Leung, E. Goodfellow, P. Ramrup, S. Woo and L. A. Cuccia, *Cryst. Growth Des.*, 2014, **14**, 1067–1076.
19 K. Soai, S. Niwa and H. Hori, *J. Chem. Soc., Chem. Commun.*, 1990, 982–983.
20 K. Soai, *Proc. Jpn. Acad., Ser. B*, 2019, **95**, 89–110.
21 M. Uwaha, *J. Phys. Soc. Jpn.*, 2004, **73**, 2601–2603.
22 M. Uwaha, *J. Phys. Soc. Jpn.*, 2008, **77**, 083802.
23 M. Uwaha and H. Katsuno, *J. Phys. Soc. Jpn.*, 2009, **78**, 023601.
24 J. M. McBride and J. C. Tully, *Nature*, 2008, **452**, 161–162.
25 Y. Saito and H. Hyuga, *J. Phys. Soc. Jpn.*, 2010, **79**, 083002.
26 Y. Saito and H. Hyuga, *J. Phys. Soc. Jpn.*, 2008, **77**, 113001.
27 Y. Saito, T. Sugimori and H. Hyuga, *J. Phys. Soc. Jpn.*, 2007, **76**, 044802.
28 A. R. Hochstim, *Origins Life Evol. Biospheres*, 1975, **6**, 317–366.
29 J. M. Ribó and D. Hochberg, *Symmetry*, 2019, **11**, 814.
30 Y. Chen and W. Ma, *PLoS Comput. Biol.*, 2020, **16**, e1007592.
31 R. D. Bourdon-García, J. Ágreda, J. Burgos-Salcedo, D. Hochberg, J. M. Ribó, P. Bargueño and A. E. Salamanca, *Phys. Chem. Chem. Phys.*, 2022, **24**, 20788–20802.
32 D. Kondepudi and L. Kapcha, *Chirality*, 2008, **20**, 524–528.
33 D. Hochberg and M.-P. Zorzano, *Chem. Phys. Lett.*, 2006, **431**, 185–189.
34 K. Suwannasang, G. Coquerel, C. Rougeot and A. E. Flood, *Chem. Eng. Technol.*, 2014, **37**, 1329–1339.
35 C. Blanco, J. M. Ribó and D. Hochberg, *Phys. Rev. E: Stat., Nonlinear, Soft Matter Phys.*, 2015, **91**, 022801.
36 D. Hochberg, A. S. Torralba and F. Morán, *Phys. Chem. Chem. Phys.*, 2020, **22**, 27214–27223.
37 Y. Saito and H. Hyuga, *J. Phys. Soc. Jpn.*, 2004, **73**, 33–35.
38 F. C. Frank, *Biochim. Biophys. Acta*, 1953, **11**, 459–463.
39 D. K. Kondepudi and G. W. Nelson, *Phys. Rev. Lett.*, 1983, **50**, 1023–1026.
40 D. K. Kondepudi and G. W. Nelson, *Phys. A*, 1984, **125**, 465–496.
41 D. K. Kondepudi, *BioSystems*, 1987, **20**, 75–83.
42 R. Plasson and A. Brandenburg, *Origins Life Evol. Biospheres*, 2010, **40**, 93–110.
43 A. Brandenburg and T. Multamäki, *Int. J. Astrobiol.*, 2004, **3**, 209–219.
44 M. Gleiser, *Origins Life Evol. Biospheres*, 2007, **37**, 235–251.
45 M. Gleiser and S. I. Walker, *Origins Life Evol. Biospheres*, 2009, **39**, 479–493.
46 D. K. Kondepudi and G. W. Nelson, *Nature*, 1985, **314**, 438–441.
47 R. Plasson, D. K. Kondepudi, H. Bersini, A. Commeyras and K. Asakura, *Chirality*, 2007, **19**, 589–600.
48 J. M. Ribó, D. Hochberg, J. Crusats, Z. El-Hachemi and A. Moyano, *J. R. Soc., Interface*, 2017, **14**, 20170699.
49 S. A. Kauffman, *J. Theor. Biol.*, 1986, **119**, 1–24.
50 M. Eigen, J. McCaskill and P. Schuster, *Advances in Chemical Physics*, John Wiley & Sons, Ltd, 1989, pp. 149–263.
51 W. Hordijk, J. Hein and M. Steel, *Entropy*, 2010, **12**, 1733–1742.
52 J. M. Ribó, C. Blanco, J. Crusats, Z. El-Hachemi, D. Hochberg and A. Moyano, *Chem. – Eur. J.*, 2014, **20**, 17250–17271.
53 C. Blanco and I. A. Chen, in *Prebiotic Chemistry and Chemical Evolution of Nucleic Acids*, ed. C. Menor-Salván, Springer International Publishing, Cham, 2018, pp. 245–261.
54 R. R. E. Steendam, J. M. M. Verkade, T. J. B. van Benthem, H. Meekes, W. J. P. van Enckevort, J. Raap, F. P. J. T. Rutjes and E. Vlieg, *Nat. Commun.*, 2014, **5**, 5543.
55 D. Frezzato, C. Zannoni and G. J. Moro, *J. Chem. Phys.*, 2006, **125**, 104903.
56 J. Jiang and D.-K. Yang, *Phys. Rev. Appl.*, 2017, **7**, 014014.
57 Y. Shin, Q. Wang and D.-K. Yang, *Soft Matter*, 2020, **16**, 3669–3677.